Breaking $\sum m_\nu$ Parameter Degeneracies with the Bispectrum

ChangHoon Hahn,[1, 2, *] Francisco Villaescusa-Navarro,[3] Emanuele Castorina,[2, 1] and Roman Scoccimarro[4]

[1]*Lawrence Berkeley National Laboratory, 1 Cyclotron Rd, Berkeley CA 94720, USA*
[2]*Berkeley Center for Cosmological Physics, University of California, Berkeley, CA 94720, USA*
[3]*Center for Computational Astrophysics, Flatiron Institute, 162 5th Avenue, New York, NY 10010, USA*
[4]*Center for Cosmology and Particle Physics, Department of Physics, New York University, NY 10003, New York, USA*

(Dated: `DRAFT --- 1ccf733 --- 2019-03-13 --- NOT READY FOR DISTRIBUTION`)

ABSTRACT

abstract

Keywords: cosmology: —

1. INTRODUCTION

very brief into on neutrinos

Brief intro on the impact of massive active neutrinos on the matter powerspectrum and how that's detectable with CMB and LSS

Quick summary of current constraints and where they come from. Talk about the CMB-LSS lever arm. The degeneracy between As and tau and how that's a bottleneck short thing about how τ is hard to constrain.

Fortunately the imprint of neutrinos on the matter distribution leaves imprints on clustering. So with clustering measurements alone we can derive constraints on $\sum m_\nu$ and at the very least tighten constraints.

Brief summary of previous works that look at the powerspectrum. Then Discuss the shortcomings of the powerspectrum only analysis– Not good enough.

However, we don't have to settle for just two point statistics, three-point statistics such as the bispectrum and 3PCF...

In Section blah

2. HADES AND QUIJOTE SIMULATION SUITES

We use a subset of the HADES[1] and Quijote simulation suites. Below, we briefly describe these simulations; a brief summary of the simulations can be found in Table 1. The HADES simulations start from Zel'dovich approximated initial conditions generated at $z = 99$ using the Zennaro
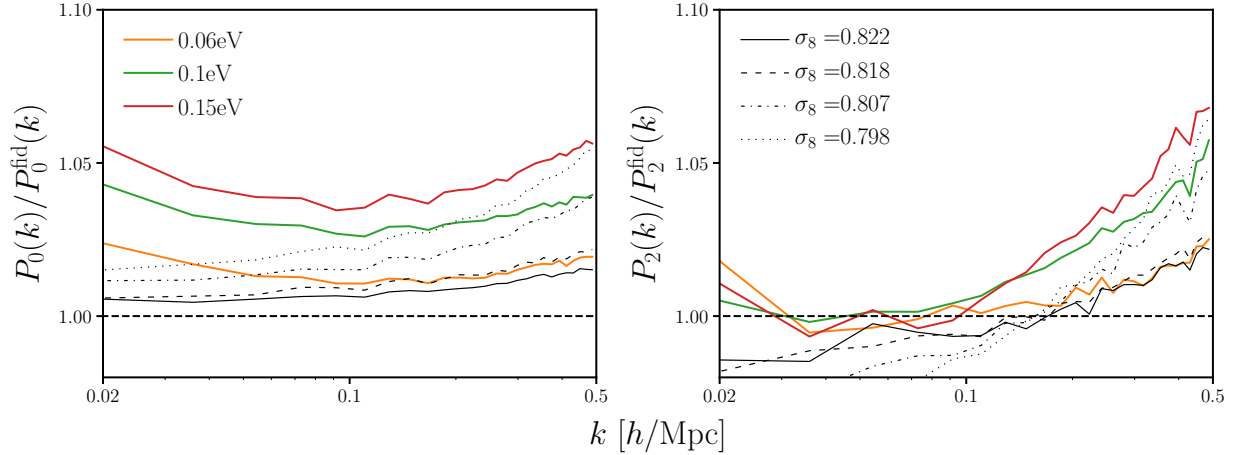

Figure 1. Impact of $\sum m_\nu$ and σ_8 on the redshift-space halo power spectrum monopole and quadrupole measured using the HADES simulation suite. $\sum m_\nu$ and σ_8 produce almost identical effects on halo clustering on small scales ($k > 0.1\,h/\mathrm{Mpc}$). This degeneracy can be partially broken through the quadrupole; however, $\sum m_\nu$ *and* σ_8 *produce almost the same effect on two-point clustering — within a few percent.*

et al. (2017) rescaling method and follow the gravitational evolution of $N_{\mathrm{cdm}} = 512^3$ CDM, plus $N_\nu = 512^3$ neutrino particles (for massive neutrino models), to $z = 0$. They are run using the GADGET-III TreePM+SPH code (Springel 2005) in a periodic $(1h^{-1}\mathrm{Gpc})^3$ box. All of the HADES simulations share the following cosmological parameter values, which are in good agreement with Planck constraints Ade et al. (2016): $\Omega_{\mathrm{m}}=0.3175, \Omega_{\mathrm{b}}=0.049, \Omega_\Lambda=0.6825, n_s=0.9624, h=0.6711$, and $k_{\mathrm{pivot}} = 0.05\ h\mathrm{Mpc}^{-1}$.

The HADES suite includes models with degenerate massive neutrinos of different masses: $\sum m_\nu = 0.06, 0.10$, and 0.15 eV. These massive neutrino models are run using the "particle method", where neutrinos are described as a collisionless and pressureless fluid and therefore modeled as particles, same as CDM (Brandbyge et al. 2008; Viel et al. 2010). HADES also includes models with massless neutrino and different values of σ_8 to examine the $\sum m_\nu - \sigma_8$ degeneracy. The σ_8 values were chosen to match either σ_8^m or σ_8^c — σ_8 computed with respect to total matter (CDM + baryons + ν) or CDM + baryons — of the massive neutrino models: $\sigma_8 = 0.822, 0.818, 0.807$, and 0.798. Each model has 100 independent realizations and we focus on the snapshots saved at $z = 0$. Halos closely trace the CDM+baryon field rather than the total matter field and neutrinos have negligible contribution to halo masses (*e.g.* Ichiki & Takada 2012; Castorina et al. 2014; LoVerde 2014; Villaescusa-Navarro et al. 2014). Hence, dark matter halos are identified in each realization using the Friends-of-Friends algorithm (FoF; Davis et al. 1985) with linking length $b = 0.2$ on the CDM + baryon distribution; only halos with masses $> 3.2 \times 10^{13} h^{-1} M_\odot$ are included. For further details on the HADES simulations, we refer readers to Villaescusa-Navarro et al. (2018).

CH: describe quijote simulations

3. BISPECTRUM

Table 1. Specifications of the HADES and Quijote simulation suites.

Name	$\sum m_\nu$ (eV)	Ω_m	Ω_b	h	n_s	σ_8^m	σ_8^c	$m_{\rm cdm}$ $(10^{10}h^{-1}M_\odot)$	m_ν $(10^{10}h^{-1}M_\odot)$	realizations
					HADES suite					
Fiducial	0.0	0.3175	0.049	0.6711	0.9624	0.833	0.833	65.66	0	100
	0.06	0.3175	0.049	0.6711	0.9624	0.819	0.822	65.36	29.57	100
	0.10	0.3175	0.049	0.6711	0.9624	0.809	0.815	65.16	49.28	100
	0.15	0.3175	0.049	0.6711	0.9624	0.798	0.806	64.92	73.95	100
	0.0	0.3175	0.049	0.6711	0.9624	0.822	0.822	65.66	0	100
	0.0	0.3175	0.049	0.6711	0.9624	0.818	0.818	65.66	0	100
	0.0	0.3175	0.049	0.6711	0.9624	0.807	0.807	65.66	0	100
	0.0	0.3175	0.049	0.6711	0.9624	0.798	0.798	65.66	0	100
					Qujiote suite					
Fiducial	0.0	0.3175	0.049	0.6711	0.9624	0.834	0.834			15,000
$\sum m_\nu^+$	<u>0.1</u>	0.3175	0.049	0.6711	0.9624	0.834	0.834			500
$\sum m_\nu^{++}$	<u>0.2</u>	0.3175	0.049	0.6711	0.9624	0.834	0.834			500
$\sum m_\nu^{+++}$	<u>0.4</u>	0.3175	0.049	0.6711	0.9624	0.834	0.834			500
Ω_m^+	0.0	<u>0.3275</u>	0.049	0.6711	0.9624	0.834	0.834			500
Ω_m^-	0.0	<u>0.3075</u>	0.049	0.6711	0.9624	0.834	0.834			500
Ω_b^+	0.0	0.3175	<u>0.050</u>	0.6711	0.9624	0.834	0.834			500
Ω_b^-	0.0	0.3175	<u>0.048</u>	0.6711	0.9624	0.834	0.834			500
h^+	0.0	0.3175	0.049	<u>0.6911</u>	0.9624	0.834	0.834			500
h^-	0.0	0.3175	0.049	<u>0.6511</u>	0.9624	0.834	0.834			500
n_s^+	0.0	0.3175	0.049	0.6711	<u>0.9824</u>	0.834	0.834			500
n_s^-	0.0	0.3175	0.049	0.6711	<u>0.9424</u>	0.834	0.834			500
σ_8^+	0.0	0.3175	0.049	0.6711	0.9624	<u>0.849</u>	<u>0.849</u>			500
σ_8^-	0.0	0.3175	0.049	0.6711	0.9624	<u>0.819</u>	<u>0.819</u>			500

Notes: CH: description of the table

   We're interested in breaking parameter degeneracies that limit the constraining power on $\sum m_\nu$ of two-point clustering analyses using three-point clustering statistics — *i.e.* the bispectrum. In this section, we describe the bispectrum estimator used throughout the paper. We focus on the bispectrum monopole ($\ell = 0$) and use an estimator that exploits Fast Fourier Transpforms (FFTs). Our estimator is similar to the estimators described in Scoccimarro (2015); Sefusatti et al. (2016); we also follow their formalism in our description below. Although Sefusatti et al. (2016) and Scoccimarro

(2015) respectively describe estimators in redshift- and real-space, since we focus on the bispectrum monopole, we note that there is no difference.

To measure the bispectrum of our halo catalogs, we begin by interpolating the halo positions to a grid, $\delta(\boldsymbol{x})$ and Fourier transforming the grid to get $\delta(\boldsymbol{k})$. We use a fourth-order interpolation to interlaced grids, which has advantageous anti-aliasing properties (?Sefusatti et al. 2016) that allow unbias measurements up to the Nyquist frequency. Then using $\delta(\boldsymbol{k})$, we measure the bispectrum monopole as

$$\widehat{B}_{\ell=0}(k_1, k_2, k_3) = \frac{1}{V_B} \int_{k_1} \mathrm{d}^3 q_1 \int_{k_2} \mathrm{d}^3 q_2 \int_{k_3} \mathrm{d}^3 q_3 \, \delta_{\mathrm{D}}(\boldsymbol{q}_{123}) \, \delta(\boldsymbol{q}_1) \, \delta(\boldsymbol{q}_2) \, \delta(\boldsymbol{q}_3) - B^{\mathrm{SN}}_{\ell=0} \tag{1}$$

δ_{D} above is a Dirac delta function and hence $\delta_{\mathrm{D}}(\boldsymbol{q}_{123}) = \delta_{\mathrm{D}}(\boldsymbol{q}_1 + \boldsymbol{q}_2 + \boldsymbol{q}_3)$ ensures that the $\boldsymbol{q}_i$ triplet actually form a closed triangle. Each of the integrals above represent an integral over a spherical shell in k-space with radius δk centered at $\boldsymbol{k}_i$ — i.e.

$$\int_{k_i} \mathrm{d}^3 q \equiv \int_{k_i - \delta k/2}^{k_i + \delta k/2} \mathrm{d}q \, q^2 \int \mathrm{d}\Omega. \tag{2}$$

V_B is a normalization factor proportional to the number of triplets $\boldsymbol{q}_1$, $\boldsymbol{q}_2$, and $\boldsymbol{q}_3$ that can be found in the triangle bin defined by k_1, k_2, and k_3 with width δk:

$$V_B = \int_{k_1} \mathrm{d}^3 q_1 \int_{k_2} \mathrm{d}^3 q_2 \int_{k_3} \mathrm{d}^3 q_3 \, \delta_{\mathrm{D}}(\boldsymbol{q}_{123}) \tag{3}$$

Lastly, $B^{\mathrm{SN}}_{\ell=0}$ is the correction for the Poisson shot noise, which contributes due to the self-correlation of individual objects:

$$B^{\mathrm{SN}}_{\ell=0}(k_1, k_2, k_3) = \frac{1}{\bar{n}}\big(P_0(k_1) + P_0(k_2) + P_0(k_3)\big) + \frac{1}{\bar{n}^2}. \tag{4}$$

$\bar{n}$ is the number density of objects (halos) and P_0 is the powerspectrum monopole.

In order to evaluate the integrals in Eq. 1, we take advantage of the plane-wave representation of the Dirac delta function and rewrite the equation as

$$\widehat{B}_{\ell=0}(k_1, k_2, k_3) = \frac{1}{V_B} \int \frac{\mathrm{d}^3 x}{(2\pi)^3} \int_{k_1} \mathrm{d}^3 q_1 \int_{k_2} \mathrm{d}^3 q_2 \int_{k_3} \mathrm{d}^3 q_3 \, \delta(\boldsymbol{q}_1) \, \delta(\boldsymbol{q}_2) \, \delta(\boldsymbol{q}_3) \, e^{i\boldsymbol{q}_{123}\cdot\boldsymbol{x}} - B^{\mathrm{SN}}_{\ell=0} \tag{5}$$

$$= \frac{1}{V_B} \int \frac{\mathrm{d}^3 x}{(2\pi)^3} \prod_{i=1}^{3} I_{k_i}(\boldsymbol{x}) - B^{\mathrm{SN}}_{\ell=0} \tag{6}$$

where

$$I_{k_i}(\boldsymbol{x}) = \int_{k} \mathrm{d}^3 q \, \delta(\boldsymbol{q}) \, e^{i\boldsymbol{q}\cdot\boldsymbol{x}}. \tag{7}$$

At this point, we measure $\widehat{B}_{\ell=0}(k_1, k_2, k_3)$ by calcuating the I_{k_i}s with inverse FFTs and summing over in real space.

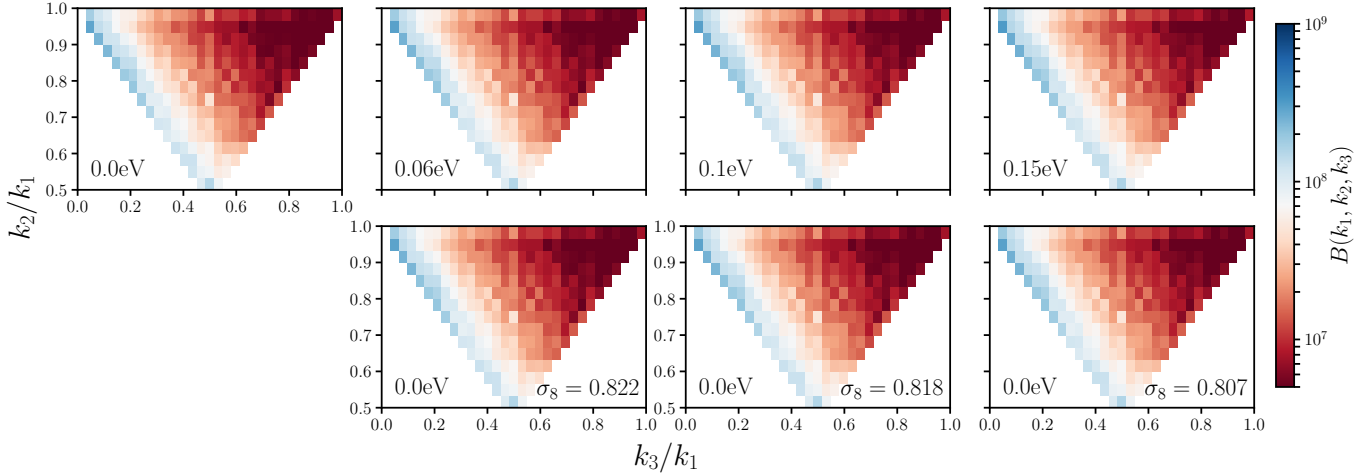We present the bispectrum measured using the estimator above in Figures 2 and 3.

Figure 2. The redshift-space halo bispectrum, $B(k_1, k_2, k_3)$ as a function of triangle configuration shape for $\sum m_\nu = 0.0, 0.06, 0.10$, and $0.15\,\mathrm{eV}$ (upper panels) and $\sigma_8 = 0.822, 0.818$, and 0.807 (lower panels). We describe the triangle configuration shape by the ratio of the triangle sides: k_3/k_1 and k_2/k_1. In each of the panels, the upper left bin contains squeezed triangles ($k_1 = k_2 \gg k_3$); the upper right bin contains equilateral triangles ($k_1 = k_2 = k_3$); and the bottom center bin contains folded triangles ($k_1 = 2k_2 = 2k_3$). We include all triangle configurations with $k_1, k_2, k_3 \leq k_{\mathrm{max}} = 0.5\,h/\mathrm{Mpc}$. In the three right-most columns, the HADES simulations of the top and bottom panels have matching σ_8 values. We describe the estimator used to calculate $B(k_1, k_2, k_3)$ in Section 3.

4. RESULTS

4.1. *Breaking the $\sum m_\nu - \sigma_8$ degeneracy*

4.2. *Forecasts*

5. SUMMARY

ACKNOWLEDGEMENTS

It's a pleasure to thank Simone Ferraro, Shirley Ho,

APPENDIX

A. REDSHIFT-SPACE BISPECTRUM

B. TESTING CONVERGENCE

REFERENCES

Ade, P. a. R., Aghanim, N., Arnaud, M., et al. 2016, Astronomy & Astrophysics, 594, A13

Brandbyge, J., Hannestad, S., Haugbølle, T., & Thomsen, B. 2008, Journal of Cosmology and Astro-Particle Physics, 08, 020

Castorina, E., Sefusatti, E., Sheth, R. K., Villaescusa-Navarro, F., & Viel, M. 2014, Journal of Cosmology and Astro-Particle Physics, 02, 049
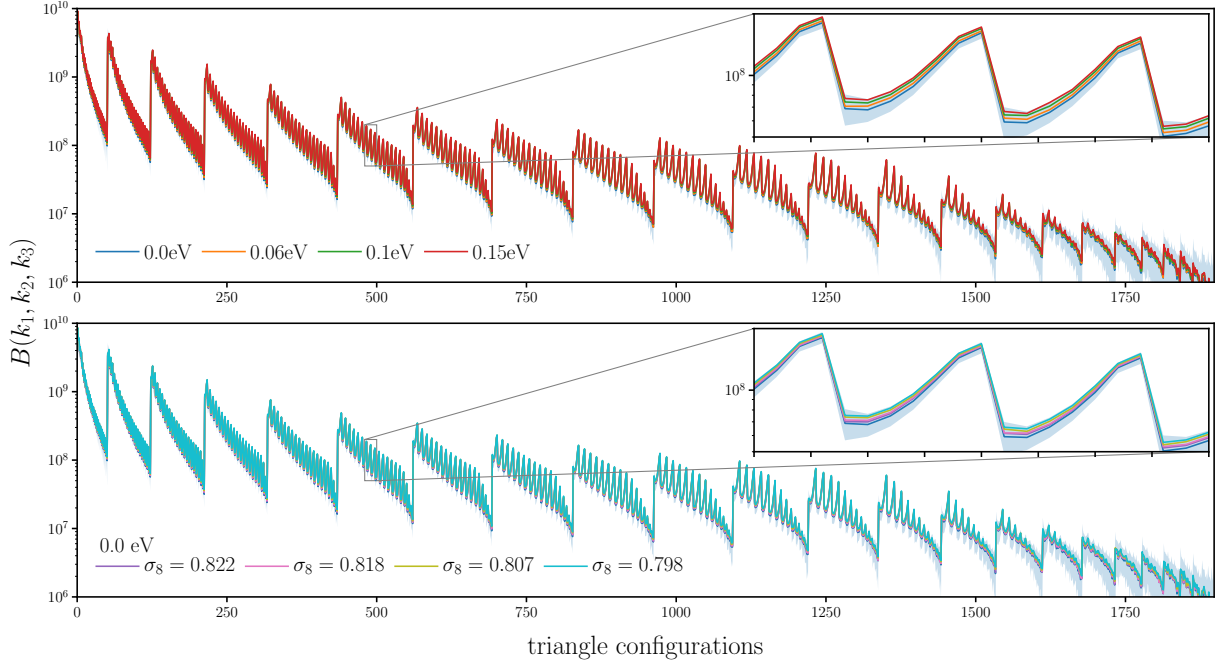
Figure 3. The redshift-space halo bispectrum, $B(k_1, k_2, k_3)$, as a function of triangle configurations for $\sum m_\nu = 0.0, 0.06, 0.10$, and 0.15 eV (top panel) and $\sum m_\nu = 0.0$ eV, $\sigma_8 = 0.822, 0.818, 0.807$, and 0.798 (lower panel). We include all possible triangle configurations with $k_1, k_2, k_3 \leq k_{\max} = 0.5$ $h/$Mpc where we loop through the configurations with k_3 in the inner most loop and k_1 in the outer most loop satisfying $k_1 \leq k_2 \leq k_3$. In the insets of the panels we zoom into triangle configurations with $k_1 = 0.113$, $0.226 \leq k_2 \leq 0.283$, and $0.283 \leq k_3 \leq 0.377$ $h/$Mpc. The blue shaded regions represent the uncertainties estimated using the 15,000 fiducial Quijote simulations and illustrate how triangle configurations on small scales are dominated by shot noise.

Davis, M., Efstathiou, G., Frenk, C. S., & White, S. D. M. 1985, The Astrophysical Journal, 292, 371

Ichiki, K., & Takada, M. 2012, Physical Review D, 85, 063521

LoVerde, M. 2014, Physical Review D, 90, 083518

Scoccimarro, R. 2015, Physical Review D, 92, arXiv:1506.02729

Sefusatti, E., Crocce, M., Scoccimarro, R., & Couchman, H. M. P. 2016, Monthly Notices of the Royal Astronomical Society, 460, 3624

Springel, V. 2005, Monthly Notices of the Royal Astronomical Society, 364, 1105

Viel, M., Haehnelt, M. G., & Springel, V. 2010, Journal of Cosmology and Astro-Particle Physics, 06, 015

Villaescusa-Navarro, F., Banerjee, A., Dalal, N., et al. 2018, The Astrophysical Journal, 861, 53

Villaescusa-Navarro, F., Marulli, F., Viel, M., et al. 2014, Journal of Cosmology and Astro-Particle Physics, 03, 011

Zennaro, M., Bel, J., Villaescusa-Navarro, F., et al. 2017, Monthly Notices of the Royal Astronomical Society, 466, 3244
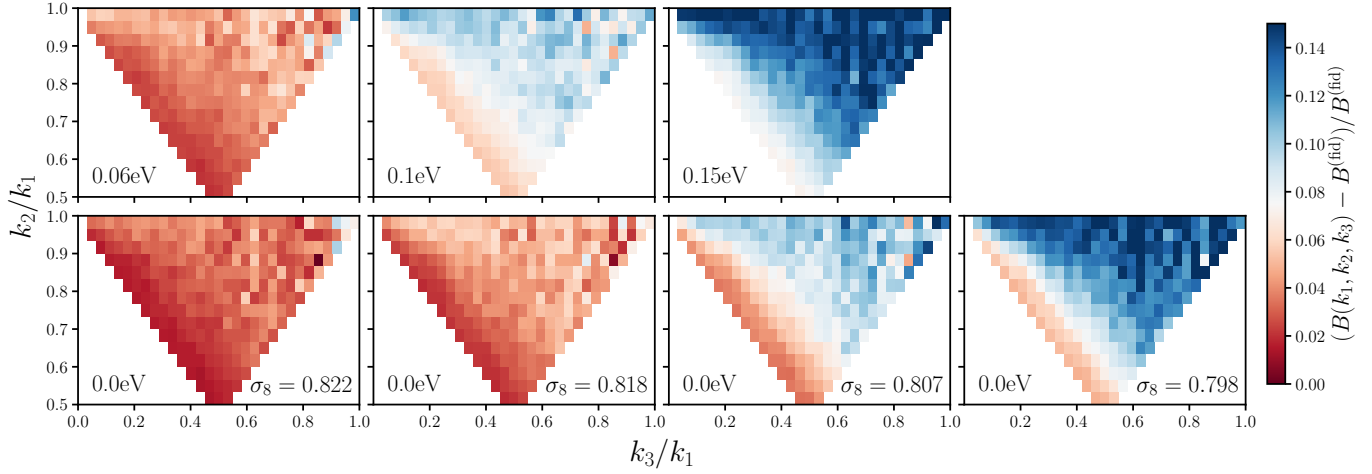
Figure 4. The shape dependence of the $\sum m_\nu$ and σ_8 imprint on the redshift-space halo bispectrum, $\Delta B/B^{\rm (fid)}$. We align the $\sum m_\nu = 0.06, 0.10,$ and $0.15\,{\rm eV}$ (upper panels) with $\sum m_\nu = 0.0$ eV, $\sigma_8 = 0.822$, 0.818, and 0.807 (bottom panels) such that simulations of top and bottom panels in each of the three columns have matching σ_8^c, which produce mostly degenerate imprints on the redshift-space power spectrum. The difference between the top and bottom panels highlight, for instance, that $\sum m_\nu$ leaves a distinct imprint on elongated and isosceles triangles (bins along the bottom left and bottom right edges, respectively) from σ_8. *The imprint of $\sum m_\nu$ has an overall distinct shape dependence on the bispectrum that cannot be replicated by a change of σ_8.*
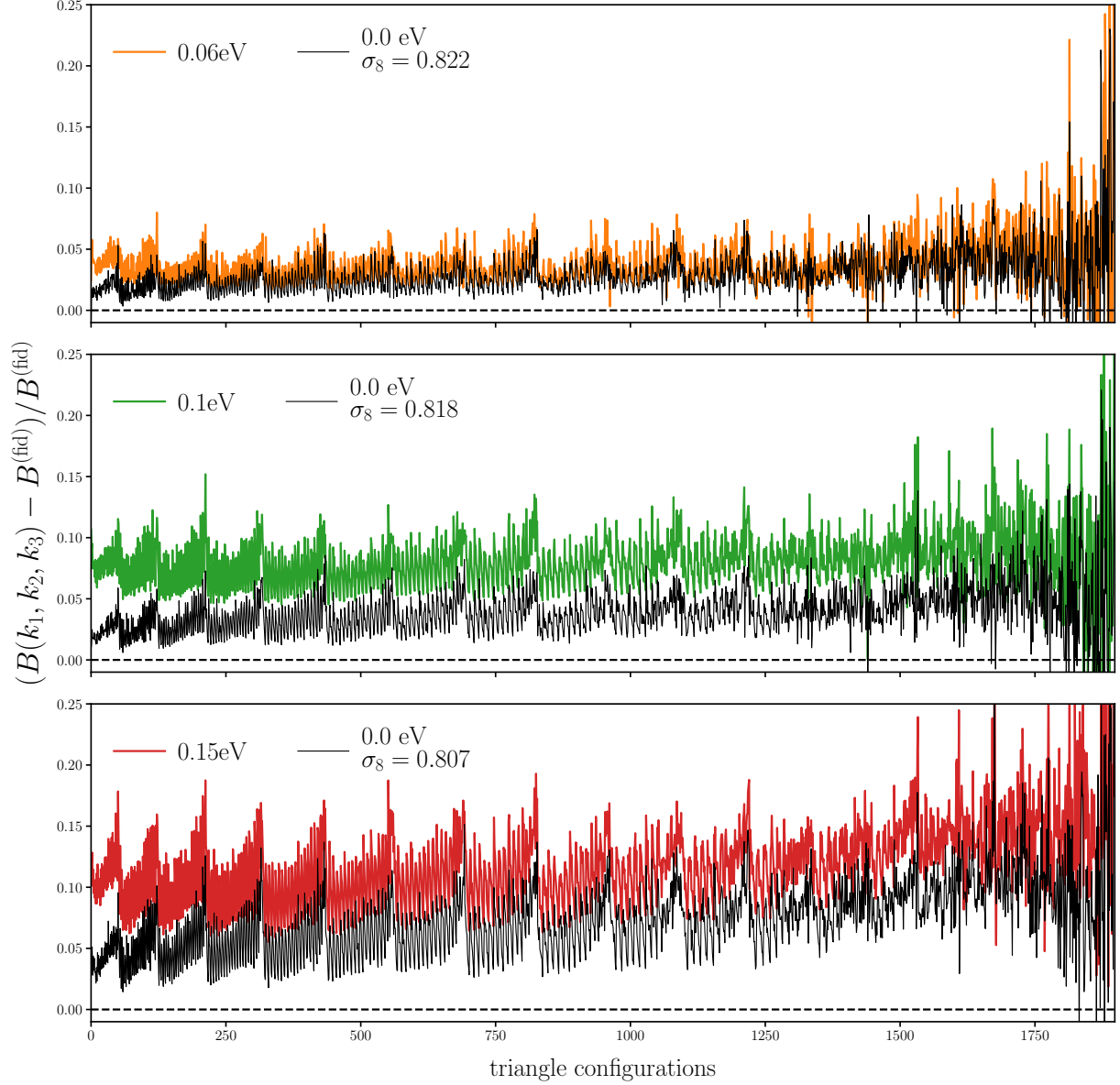
Figure 5. The impact of $\sum m_\nu$ and σ_8 on the redshift-space halo bispectrum, $\Delta B/B^{(\text{fid})}$, for triangle configurations with $k_1, k_2, k_3 \leq 0.5h$/Mpc. We compare $\Delta B/B^{(\text{fid})}$ of the HADES simulations with $\sum m_\nu = 0.06$ (top), 0.10 (middle), and 0.15 eV (bottom) to $\Delta B/B^{(\text{fid})}$ of $\sum m_\nu = 0.0$ eV HADES simulations with matching σ_8. The impact of $\sum m_\nu$ on the bispectrum has a significantly different amplitude than the impact of σ_8. For instance, $\sum m_\nu = 0.15$ eV (red) has a $\sim 5\%$ stronger impact on the bispectrum than $\sum m_\nu = 0.0$ eV, $\sigma_8 = 0.798$ (black). Meanwhile, these two simulations have power spectrums that differ by $< 1\%$ (Figure 1). Combined with the shape-dependence of Figure 4, *the distinct impact of $\sum m_\nu$ and σ_8 on the redshift-space halo bispectrum illustrate that the bispectrum can break the degeneracy between $\sum m_\nu$ and σ_8 that degrade constraints from two-point analyses.*
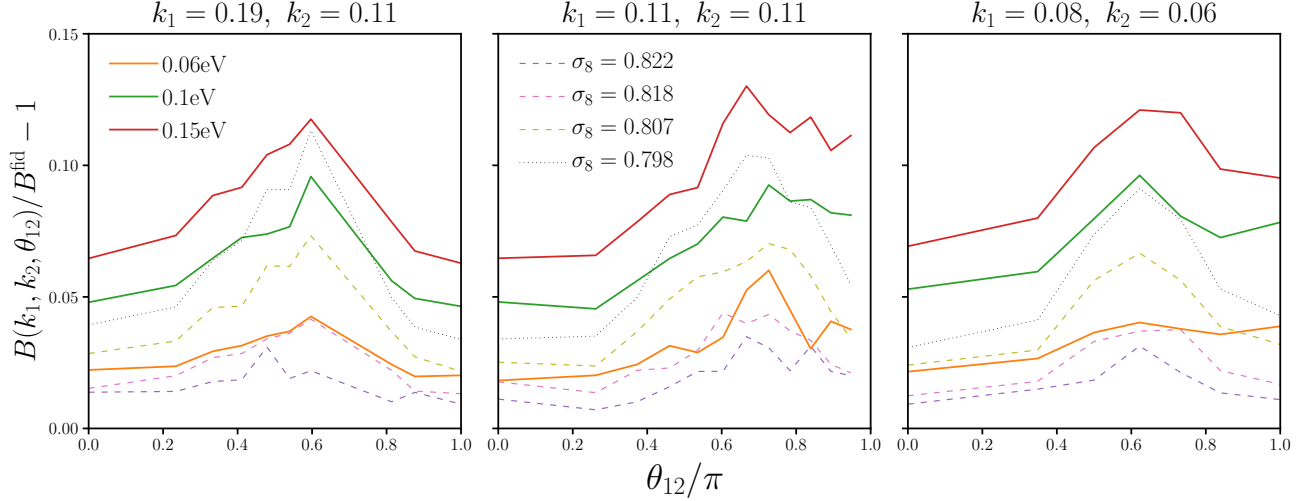
Figure 6. The impact of $\sum m_\nu$ and σ_8 on the redshift-space halo bispectrum, $\Delta B/B^{(\mathrm{fid})}$, for triangles that have $[k_1, k_2] = [0.19, 0.11], [0.11, 0.11]$ and $[0.08, 0.06]$ h/Mpc (left to right) with different angles in between, θ_{12}. Again, the HADES simulations with $\sum m_\nu = 0.06, 0.10$, and 0.15 eV (orange, green, red) have matching σ_8^c with the $\sum m_\nu = 0.0$ eV, $\sigma_8 = 0.822, 0.818$, and 0.807 (purple, pink, yellow dashed). Comparison between these two sets of simulations further illustrate the distinct imprint of the $\sum m_\nu$ on the bispectrum. We also include $\sum m_\nu = 0.0$ eV, $\sigma_8 = 0.798$ (black dashed) to highlight that change in σ_8 cannot reproduce the imprint of $\sum m_\nu$.
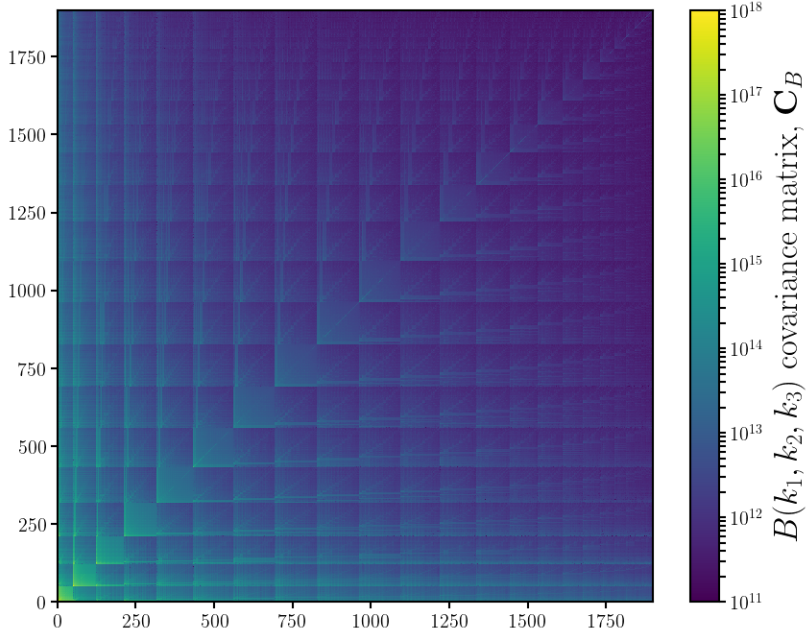
Figure 7. Covariance matrix of the redshift-space halo bispectrum estimated using the 15,000 realizations of the Qujiote simulation suite with the fiducial cosmology: $\Omega_\mathrm{m}=0.3175$, $\Omega_\mathrm{b}=0.049$, $h=0.6711$, $n_s=0.9624$, $\sigma_8=0.834$, and $\sum m_\nu=0.0$ eV. The triangle configurations (the bins) have the same ordering as in Figures 3 and 6.
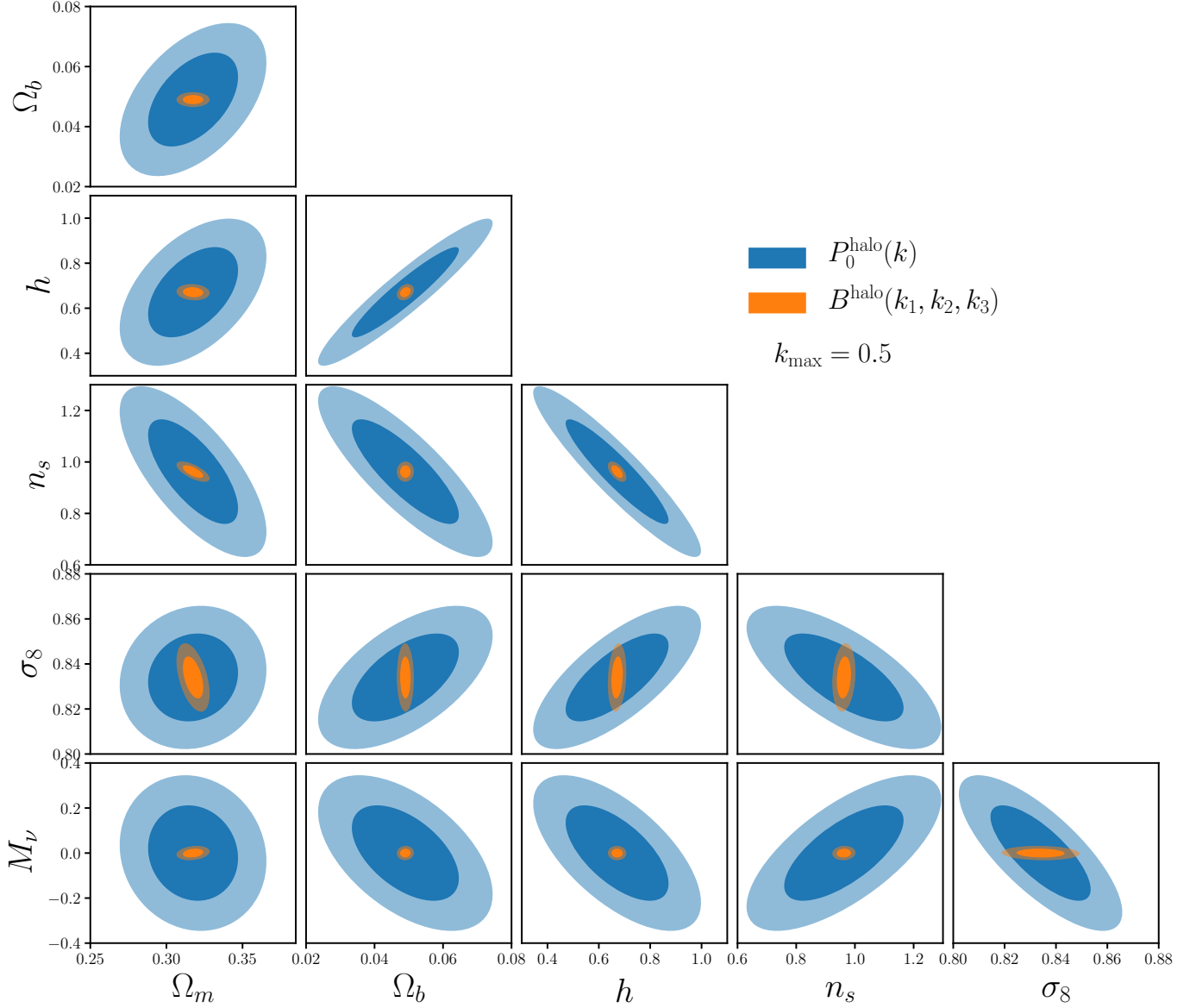
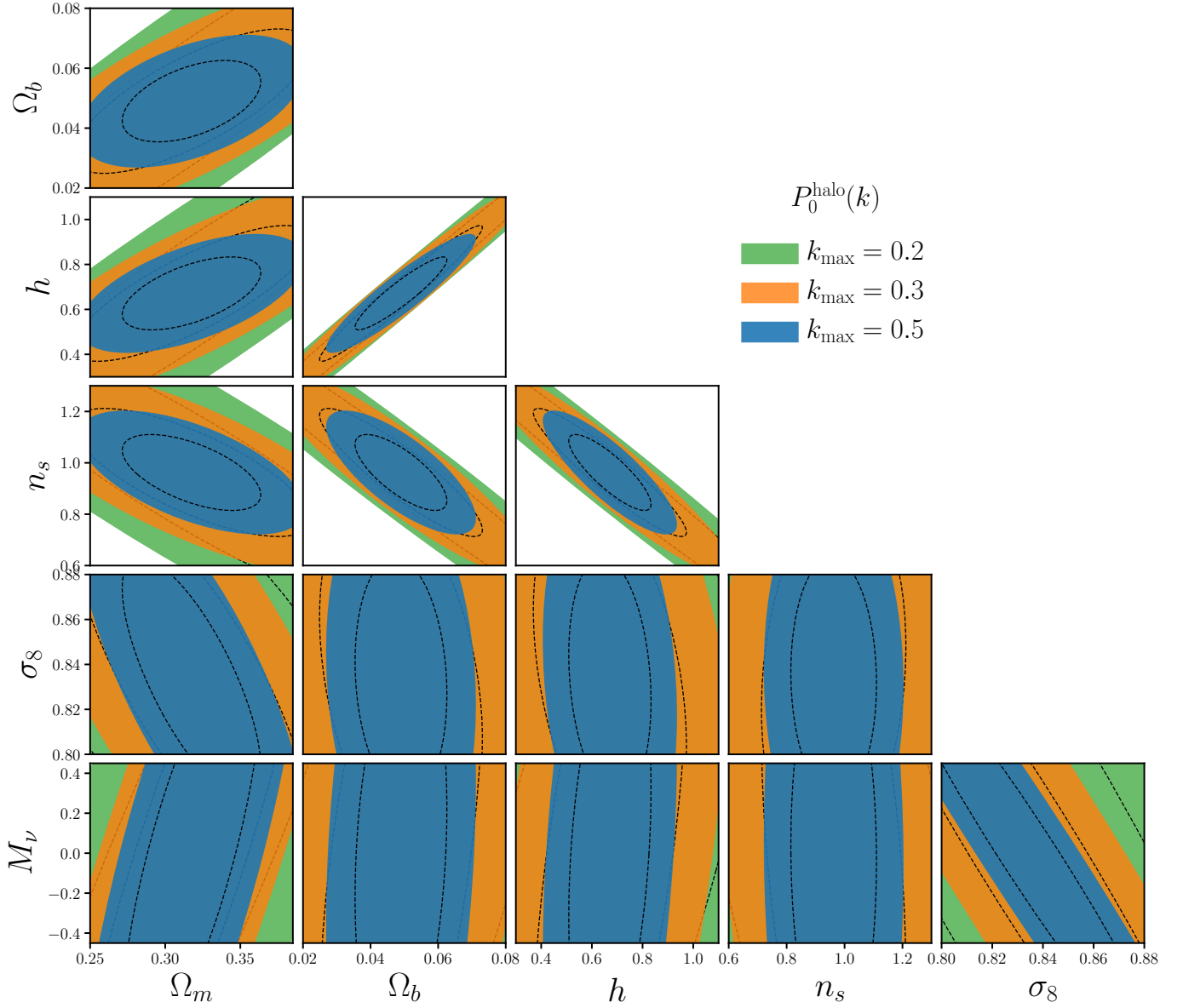**Figure 8.** Fisher forecast constraints on cosmological parameters from the redshift-space halo power spectrum monopole (blue) and bispectrum (orange) derived using the Quijote simulation suite. For both the power spectrum and bispectrum constraints, we set $k_{\mathrm{max}} = 0.5\ h/\mathrm{Mpc}$. The contours mark the 68% and 95% confidence interals. The bispectrum *substantially* improves constraints on all of the cosmological parameters over the power spectrum. *For $\sum m_\nu$, the bispectrum improves the constraint from $\sigma_{\sum m_\nu} = 0.279$ to 0.0258 — over an order of magnitude improvement over the power spectrum.*

Figure 9. Fisher forecast constraints on cosmological parameters from the redshift-space halo power spectrum monopole for $k_{\mathrm{max}} = 0.2$ (green) 0.3 (orange), and 0.5 h/Mpc (blue). The contours mark the 68% (black dashed) and 95% confidence intervals. The contours illustrate the degeneracy between $\sum m_\nu$ and σ_8 we find in the power spectrum comparisons of the HADES simulations (Figure 1).
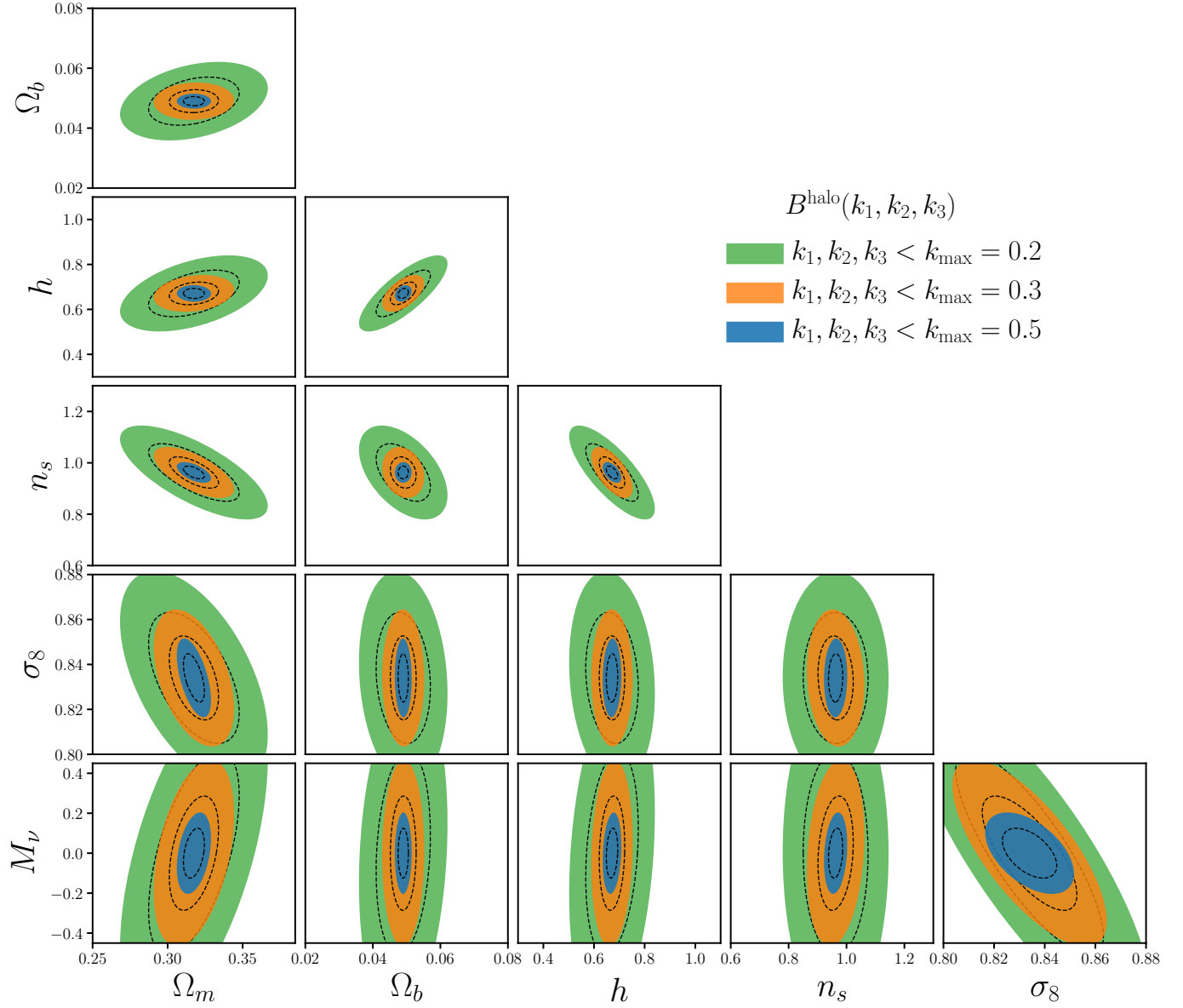
Figure 10. Constraints on cosmological parameters from the redshift-space halo bispectrum for $k_1, k_2, k_3 \leq k_{\max} = 0.2$ (green) 0.3 (orange), and 0.5 h/Mpc (blue). The contours mark the 68% (black dashed) and 95% confidence intervals. As we find with the bispectrum comparisons of the HADES simulations (Section 4.1, the bispectrum breaks the degeneracy with σ_8. **CH:** probably want to say more things
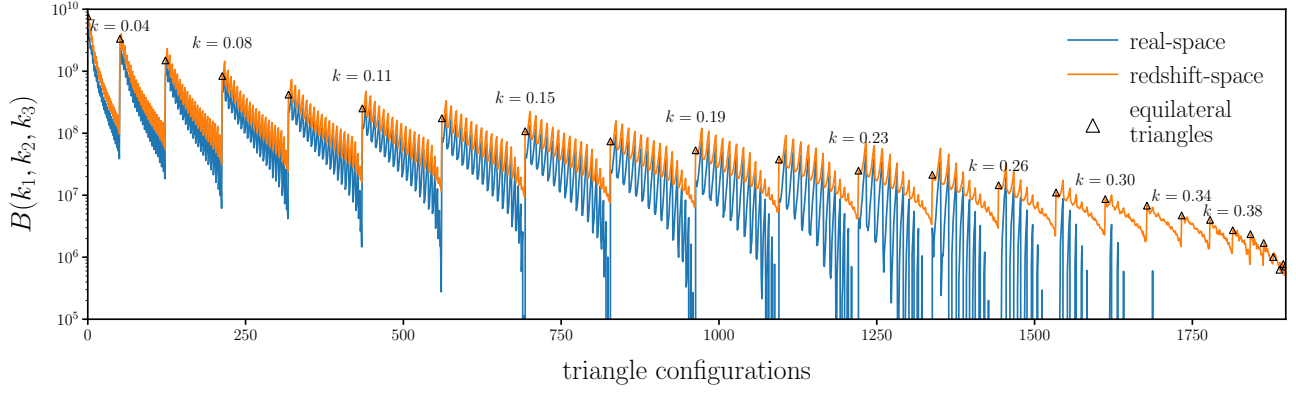
Figure 11. Comparison of the fiducial HADES simuluations real and redshift-space halo bispectrum for triangle configurations with $k_1, k_2, k_3 \leq k_{\max} = 0.5 h/\mathrm{Mpc}$ (blue and orange respectively). We mark equilateral triangle configurations (empty triangle marker) along with their side lengths k.
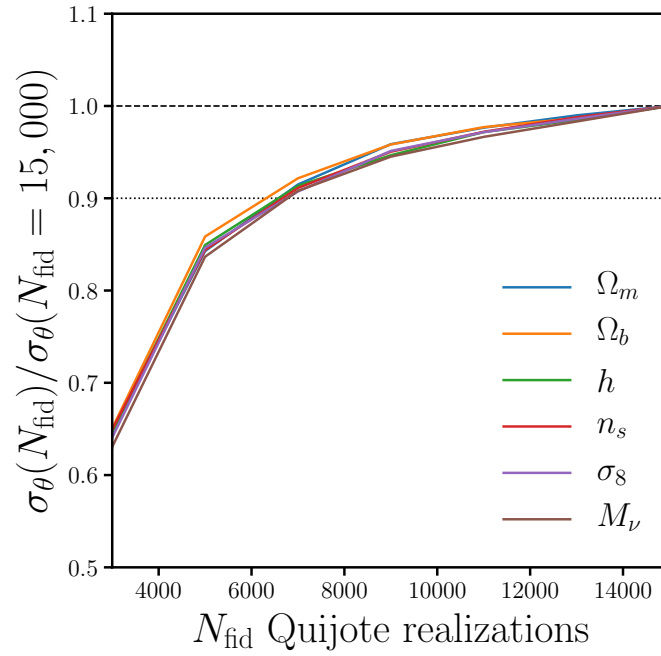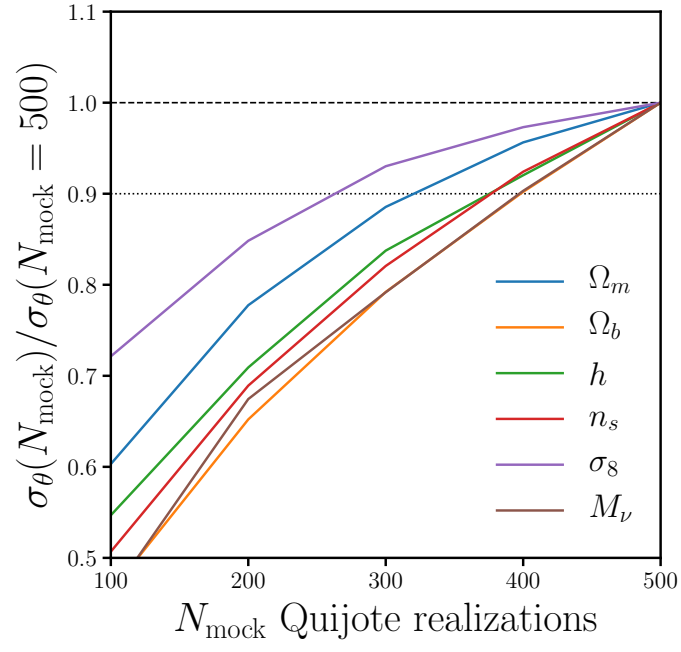

Figure 12.

Figure 13.